Preparation of high filling ratio Fe_2O_3@MWCNTs composite particles and catalytic performance on thermal decomposition of ammonium perchlorate

Wang Renpeng[1], *Li Zhaoqian*[1], *Ma Yongjun*[1,2], *Zhao Fengqi*[3], *Pei Chonghua*[1]

[1]*State Key Laboratory Cultivation Base for Nonmetal Composites and Functional Materials, Southwest University of Science and Technology, Mianyang 621010, People's Republic of China*
[2]*Analytical and Testing Center, Southwest University of Science and Technology, Mianyang 621010, People's Republic of China*
[3]*Science and Technology on Combustion and Explosion Laboratory, Xi'an Modern Chemistry Research Institute, Xi'an 710065, People's Republic of China*
E-mail: peichonghua@swust.edu.cn

Published in Micro & Nano Letters; Received on 24th June 2014; Revised on 30th August 2014; Accepted on 19th September 2014

Iron oxide-filled multi-walled carbon nanotubes (Fe_2O_3@MWCNTs) composite particles were produced by a mild and superior physical absorption method using molten $Fe(NO_3)_3{\cdot}9H_2O$ as the precursor. Characterisation of Fe_2O_3@MWCNTs composite particles was performed by X-ray diffraction, scanning electron microscopy, transmission electron microscopy and thermogravimetry-differential scanning calorimetry. The results showed a large number of hematite phase Fe_2O_3 were uniformly filled in the MWCNTs, and the mass fraction of Fe_2O_3 was about 25.8 wt%. Furthermore, in the presence of 10 wt% Fe_2O_3@MWCNTs composite particles, the peak temperature of the high-temperature decomposition of ammonium perchlorate (AP) decreased by 116°C, the peak of the low-temperature decomposition disappeared and the amount of AP heat released was increased about 200 kJ/mol.

1. Introduction: As an oxidiser, ammonium perchlorate (AP) is a major component (65–71%) of the propellant [1], of which the decomposition properties are closely related to the combustion performance of the propellant. In general, the lower the pyrolysis temperature of AP, the higher the combustion rate [2–4]. This characteristic can be obtained by adding a combustion catalyst.

Transition metal oxides as combustion catalysts have significant catalytic activities in the thermal decomposition of AP, especially in the nanoscale [5]. The catalytic activities of nanometre-sized Fe_2O_3 in the thermal decomposition of AP have been reported [6]. The catalytic performance of Fe_2O_3 is very good in rocket propellants, because of its large specific surface and plentiful reaction centres. However, nanoFe_2O_3 is prone to agglomeration. It is difficult to mix nanoFe_2O_3 with the other components of propellants. Therefore, it is very important to use nanoFe_2O_3 with good dispersibility.

As a novel carbon material, carbon nanotubes (CNTs) have attracted much attention because of their extraordinary physical and chemical properties, excellent electric conductivity, special nanostructure and nanoscale. In addition, CNTs have diameters in the nanometre range and a large internal cavity, so they are considered to be good carriers [7].

Over the past several years, metal-filled CNTs have attracted much attention because of their special electronic [8, 9], magnetic [10–12] and optical [13] properties. These materials can be used for many important applications in nanotechnology [14–18], catalytics, biomedical sciences [19, 20], memory device technology [20–25] and as electrode materials in electrochemical devices [26]. Several studies have reported the preparation of metal-filled CNTs [27–34] using two-step or one-step methods. Borowiak-Palen *et al.* [35] successfully applied wet chemistry techniques to fill single-walled CNTs (SWCNTs) continuously on a bulk scale with iron. The magnetic characterisation of the resulting Fe-filled SWCNTs revealed ferromagnetic behaviour at room temperature. Schnitzler *et al.* [36] reported a direct method for an in situ synthesis of iron and iron oxide-filled CNTs and bucky-onions, based on the pyrolysis of ferrocene or a ferrocene–$Fe_3(CO)_{12}$ mixture in a poor oxygen-containing atmosphere. Porous Vycor glass and the walls of the quartz tube of the reactor were used as the growth substrate. However, for Fe- or Fe_2O_3-filled CNTs, in addition to the main product of iron or iron oxide, compounds of iron and carbon, such as Fe_3C and Fe_3O_4, are also formed [26, 36, 37]. Hang *et al.* [26] used a chemical method to prepare Fe_2O_3-filled CNT material; the discharge capacity was improved compared to that of nanosized Fe_2O_3-loaded CNTs. The obtained material contains Fe_2O_3 and carbon without any side product; however, the level of filling with the method is not satisfactory.

The present Letter describes a novel approach to the filling of MWCNTs to prepare high filling ratio Fe_2O_3@MWCNTs nanocomposite material. $Fe(NO_3)_3{\cdot}9H_2O$, a low melting point metallic compound, was used as an iron source. This fabrication process uses the capillary effect to achieve the filling of the nanotubes. In addition, the catalytic activities of Fe_2O_3@MWCNTs in the thermal decomposition of AP were studied. Carbon material, such as activated carbon, CNT and carbon, is a type of novel catalyst on the propellant [38]. In addition, Shukla and Leszczynski [39] found that the nanocomposite catalysts in solid propellant have a synergistic catalytic effect [40, 41]. Therefore, using MWCNTs as the carrier of Fe_2O_3 not only limits the degree of freedom of nanoparticles, avoiding nanoparticle agglomeration to improve the dispersibility of Fe_2O_3, but also obtains the nanocomposite catalyst, which is beneficial for catalysing AP thermal decomposition.

2. Experimental

2.1. Materials: Pristine large-inner diameter multi-walled CNTs (MWCNTs) were prepared by the chemical vapour deposition (CVD) method on a Ni-based catalyst with an inner diameter of more than 20 nm, thickness of 5 nm and outer diameter of 30–80 nm (Chengdu Organic Chemicals Co. Ltd, Chinese Academy of Sciences). To remove the catalytic particles, we separated the MWCNTs, and dissolved the remaining oxide materials and other unprotected metal particles, and the MWCNTs were purified by following the procedure as describe elsewhere [42]: the pristine MWCNTs were ultrasonicated in concentrated HNO_3 (68%) for 2 h, neutralised with NaOH, filtered, washed with deionised water, then dried in a vacuum drying oven for 12 h

and heat treated at 450°C in N_2 atmospheres for 15 min. All chemicals, such as $Fe(NO_3)_3{\cdot}9H_2O$, sodium hydroxide (NaOH) and concentrated nitric acid (HNO_3) were of analysis reagent (AR) grade (Chengdu Kelon Chemical Reagent Factory). Deionised water was prepared in our own laboratory.

2.2. Preparation of filled samples: First, $Fe(NO_3)_3{\cdot}9H_2O$ (ca. 10 g) was added into a beaker that was placed in a thermostat water bath cauldron at 55°C (ca. 8°C above the melting point of iron nitrate nonahydrate, 47.2°C). The $Fe(NO_3)_3$ solution was obtained. Secondly, the MWCNTs (ca. 0.3462 g) were added to the Fe $(NO_3)_3$ and stirred until the MWCNTs were evenly dispersed in the solution. Then the mixture was sonicated at 59 kHz for 2 h at 55°C. After that, the mixture was continuously stirred for 36 h at 55°C. To remove the $Fe(NO_3)_3$ that was on the surface of the tubes, the sample was washed with concentrated HNO_3 until the MWCNTs were well dispersed in the acid. The MWCNTs were separated from the mixture using a centrifuge and dried at 40°C for 6 h and then at 120°C for 6 h. Finally, the sample was heated at 400°C in N_2 atmosphere for 2 h to obtain the Fe_2O_3@MWCNTs composite material.

The samples of AP containing catalysts (Fe_2O_3, Fe_2O_3 + CNTs and CNTs Fe_2O_3@MWCNTs) were made by grinding into powder. The resultant powder was analysed by X-ray diffraction (XRD), scanning electron microscopy (SEM) and transmission electron microscopy (TEM).

2.3. Characterisation: Differential scanning calorimetry (DSC) was studied by the simultaneous thermal analyser (SDT Q600 TA, USA) in N_2 atmosphere. The linear heating rate was set to different timings (5, 10 and 20°C/min) and the range was set from ambient temperature to 550°C. Thermogravimetry (TG) was studied in an air atmosphere. The linear heating rate was set at 20°C/min and the range was set from the ambient temperature to 800°C. XRD measurements were performed on XRD apparatus (X'pert PRO PANalytical, The Netherlands) scanning from 3° to 80° using Cu Kα radiation ($\lambda = 1.540598$ Å). The microstructure of the Fe_2O_3–MWCNTs composite was observed by a tungsten filament SEM (Evo 18 Carl Zeiss SMT Pte. Ltd, Germany). TEM images were measured on a TEM combined with a high-resolution TEM (HRTEM) (TEM/HRTEM, Tecnai F20, FEI, operated at 200 kV). Before TEM analysis, samples were crushed to powder, ultrasonically dispersed in the ethanol and deposited on a TEM copper grid.

3. Results and discussion: Analysis on the phases of purified MWCNTs and pristine MWCNTs were carried out by XRD. The results are shown in Fig. 1, and demonstrate that the characteristic $d_{(002)}(2\theta = 26.4°$, 41–1487) peaks of MWCNTs corresponding to cliftonite are seen in pristine as well as purified MWCNTs samples. This indicates that purified MWCNTs have the same crystal structure as the pristine MWCNTs, and the MWCNTs' structure is not destroyed after acid treatment. In addition, the peak intensities of the purified MWCNTs are narrower and higher than those of the pristine ones. The result implies that the degree of crystallisation for purified MWCNTs is superior to pristine MWCNTs and the residual amorphous carbon has been removed.

Analysis on the phases and components of the prepared Fe_2O_3@MWCNTs were carried out by XRD. Details of the XRD analysis results are shown in Fig. 2. The diffraction peak assigned to the (002) plane of MWCNTs at $2\theta = 26.4°$ can be clearly distinguished. The diffraction peaks at 24.1°, 33.1°, 35.6°, 40.8°, 49.4°, 53.99°, 62.4° and 63.96° correspond to the (012), (104), (110), (113), (024), (116), (214) and (300) crystal planes of hematite (JCPDS No. 89-0589), respectively. The results show that MWCNTs and Fe_2O_3 are both contained in the synthetic sample. In other words, the obtained material contains Fe_2O_3 and carbon without any side product.

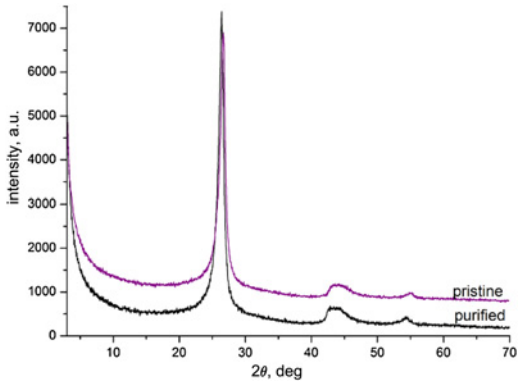

Figure 1 *XRD spectra of pristine and purified MWCNTs*

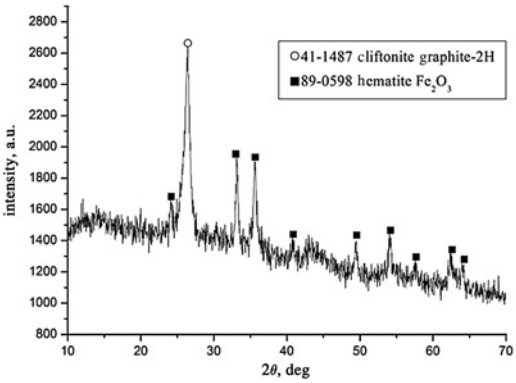

Figure 2 *XRD spectrum of the Fe_2O_3@MWCNTs*

Fig. 3 shows the SEM images of purified MWCNTs and Fe_2O_3@MWCNTs. Comparing Figs. 3*a* and *b*, we can conclude that the synthetic samples have been sufficiently washed. Fig. 3*c* is the magnified Fe_2O_3@MWCNTs morphology. From Fig. 3*c*, it can be observed that there is no residual material between the CNTs and the sample surfaces are smooth. This result indicates no deposition on the CNTs' surfaces.

TEM micrographs shown in Fig. 4 illustrate the morphology of the purified MWCNTs (Fig. 4*a*) in comparison with the Fe_2O_3@MWCNTs (Fig. 4*b*). Fig. 4*a* shows that there is nothing in the internal cavity of purified MWCNTs. From Fig. 4*b*, it can be clearly observed that most internal cavities of the MWCNTs are filled with fine Fe_2O_3 nanoparticles and the filling is continuous. In addition, the outer walls of the MWCNTs are clean, consistent with the SEM analyses. Based on the visual inspection of the whole of Fig. 4*b*, the filling ratio is estimated to be higher than ca. 90% (volume fraction). Compared to a previous study [43], the filling ratio is very high. The results of XRD, SEM and TEM suggest that the Fe_2O_3 has been uniformly and continuously filled into the internal cavity of the MWCNTs.

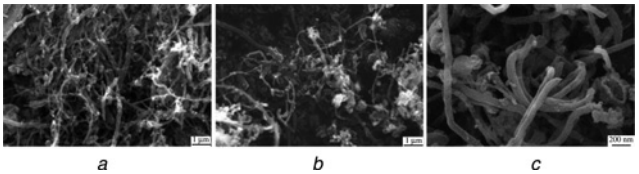

Figure 3 *SEM images*
a Purified MWCNTs
b Fe_2O_3@MWCNTs
c Magnified Fe_2O_3@MWCNTs morphology

doi: 10.1049/mnl.2014.0263

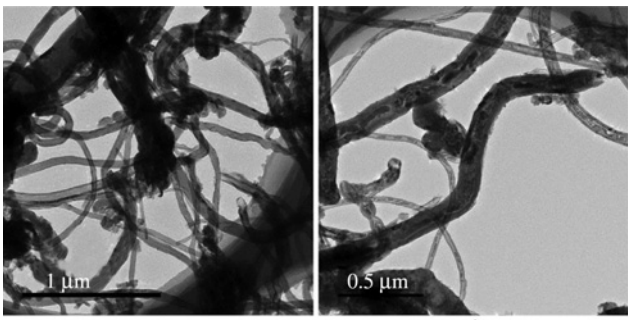

Figure 4 *TEM images*
a Purified MWCNTs
b Fe_2O_3@MWCNTs

To measure the filled amount, analysis of the Fe_2O_3@MWCNTs sample was carried out by TG. Fig. 5 provides the TG curves of Fe_2O_3@MWCNTs and MWCNTs. From the curves, it can be clearly seen that the weight loss of pure MWCNTs is 100% and the weight loss of Fe_2O_3@MWCNTs is 74.2% when the temperature is less than 700°C. When the temperature rises to more than 700, the MWCNTs will react with air, transform into gases and leave behind the Fe_2O_3. So, in the Fe_2O_3@MWCNTs sample, the mass fraction of the Fe_2O_3 is 25.8%. The result indicates that the filling rate of synthesised Fe_2O_3@MWCNTs is very high, consistent with the TEM analyses.

Using DSC analyses, five samples, after adding different amounts of Fe_2O_3@MWCNTs, were configured to investigate the influence of Fe_2O_3@MWCNT nanocomposite catalyst on the thermal decomposition behaviour of AP. The five samples are as follows: a (0 wt% Fe_2O_3@MWCNTs + AP), b (1 wt% Fe_2O_3@MWCNTs + AP), c (2 wt% Fe_2O_3@MWCNTs + AP), d (5 wt% Fe_2O_3@MWCNTs + AP) and e (10 wt% Fe_2O_3@MWCNTs + AP). The DSC curves are both in Fig. 6.

From the curve of pure AP, three peaks can be clearly observed, an endothermic peak at 252°C, a low-temperature exothermic peak at 342°C and a high-temperature exothermic peak at 450°C, respectively. The endothermic peak is attributed to the crystallographic transition of AP from orthorhombic to cubic [44, 45]. The low-temperature exothermic peak at 342°C is because of the partial decomposition of AP and formation of some intermediate NH_3 and $HClO_4$ by dissociation and sublimation [46]. The high-temperature exothermic peak at about 450°C is caused by the complete decomposition of AP into volatile products. From the curves of a, b, c, d and e, it can be clearly seen that the temperature interval between the low-temperature exothermic peak and the high-temperature exothermic peak of AP becomes smaller as the mass fraction of Fe_2O_3@MWCNTs increases. With the addition of Fe_2O_3@MWCNTs increased to 5 and 10 wt%, there is only one

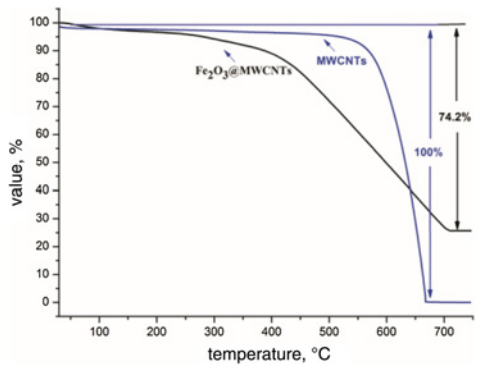

Figure 5 *TG curve of Fe_2O_3@MWCNTs and MWCNTs*

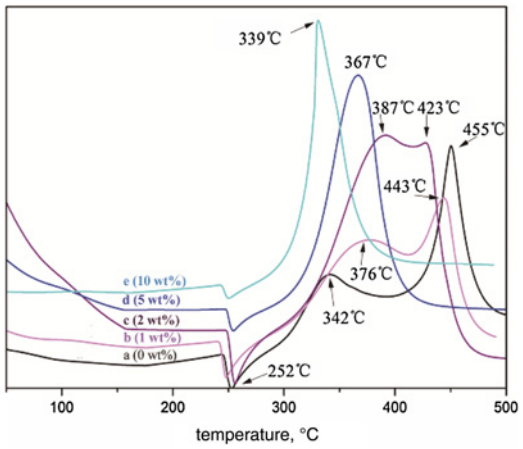

Figure 6 *DSC curves of adding different amounts of Fe_2O_3@MWCNTs to AP*

exothermic peak for the curves d and e, at 367 and 339°C, respectively. The exothermic peak after adding 10 wt% Fe_2O_3@MWCNTs is even lower than the low-temperature exothermic peak of AP. This shows that the catalytic performance of Fe_2O_3@MWCNTs on the thermal decomposition of AP is very good. In addition, the endothermic peak at 252°C occurs in all curves, which indicates that there is no distinct catalytic effect of Fe_2O_3@MWCNTs on the crystal structure transformation of AP, consistent with the previous study [47].

Table 1 shows that the ΔT value of adding 2, 5 and 10 wt% Fe_2O_3@MWCNTs is 123, 69 and 50°C, respectively. Gradual decline in the value of ΔT indicates that adding MWCNTs@Fe_2O_3 can obviously increase the rate of heat liberation of AP. That is to say, catalyst Fe_2O_3@MWCNTs can increase the decomposition rate of AP. Furthermore, the ΔH of AP adding 1, 2, 5 and 10 wt% Fe_2O_3@MWCNTs is 156.4, 258.2, 270.9, 362.4 and 356.4 kJ/mol, respectively. After adding catalyst into AP, the ΔH of AP increases significantly compared with pure AP. Especially, after adding 5 and 10 wt% catalyst into AP, the ΔH of AP increases about 200 kJ/mol. The reason may be that the narrower the AP decomposition area, the greater the release.

For the purpose of contrasting the catalytic performance of Fe_2O_3, MWCNTs, Fe_2O_3 + MWCNTs and Fe_2O_3@MWCNTs on the thermal decomposition of AP, the thermal decomposition temperatures were measured for: a mixture of 10 wt% Fe_2O_3 and AP; a mixture of 10 wt% MWCNTs and AP; a mixture of 2.57% Fe_2O_3, 7.43% MWCNTs and AP; and a mixture of AP and 10 wt% Fe_2O_3@MWCNTs composite particles. Details of the DSC analysis results are shown in Fig. 7. The curves in Fig. 7 show that the whole samples have only one decomposition peak. The peak temperature of adding Fe_2O_3, MWCNTs, Fe_2O_3 + MWCNTs and Fe_2O_3@MWCNTs is at 368, 362, 360 and 339°C, respectively. This shows that the catalytic performance of Fe_2O_3@MWCNTs

Table 1 DSC results of adding different amounts of Fe_2O_3@MWCNTs to AP

Samples	T_i, °C	ΔT, °C	T_{Max}, °C	ΔH, kJ/mol
a (0 wt%)	307–358/432–472	51/40	342/450	156.4
b (1 wt%)	313–407/423–461	94/38	376/443	258.2
c (2 wt%)	321–444	123	387	270.9
d (5 wt%)	323–392	69	367	362.4
e (10 wt%)	319–368	50	339	356.4

Note: T_i is the decomposition temperature; ΔT is the decomposition temperature range; T_{Max} is the decomposition peak temperature; and ΔH is the heat releases

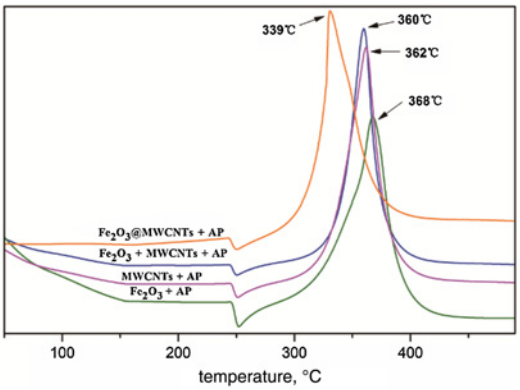

Figure 7 *DSC patterns of different samples*

on the thermal decomposition of AP is better than the catalytic performance of Fe_2O_3, MWCNTs and Fe_2O_3 + MWCNTs. In other words, the catalytic performance of Fe_2O_3 on the thermal decomposition of AP can be improved by filling with CNTs.

The kinetic parameters of the thermal decomposition of AP are calculated by the Kissinger [48] method in the following equation

$$\mathrm{Ln}(\beta/T_{\max}^2) = \mathrm{Ln}(R^*A/E_a) - E_a/RT_{\max} \quad (1)$$

where β is the heating rate (°C/min), $T_{\max}$ is the most rapidly decomposing temperature (K) and R is the gas constant. The result is shown in Table 2. The E_a of AP has reduced from 310.3 to 81.4 kJ/mol, which indicates that the catalyst has catalysed the thermal decomposition of AP.

It can be seen from the above experimental results that Fe_2O_3@MWCNTs composite material significantly catalyses the low-temperature as well as the high-temperature exothermic process of AP decomposition. The process of AP decomposition is very complex. The low-temperature decomposition is a solid–gas heterogeneous reaction, dissociation and sublimation process, whereas the high-temperature decomposition of AP is a gas-phase reaction [49]. These processes mainly contain four decomposition steps [50, 51]: (a) negative charges transfer from ClO_4^- to NH_4^+ ($ClO_4^- + NH_4^+ \leftrightarrow NH_4 + ClO_4$); (b) positive charges transfer from NH_4^+ to ClO_4^- ($ClO_4^- + NH_4^+ \leftrightarrow NH_3 + HClO_4$); (c) $ClO4^-$ decomposition ($ClO_4^- \leftrightarrow ClO_3^- + O$); and (d) NH_3 oxidation ($NH_3 + 2O \leftrightarrow HNO + H_2O$). As is well known, the reason why the low-temperature decomposition of AP is terminated is that the early decomposition generated NH_3 covers the activation centre of the AP. This 'deactivation' of NH_3 is because it inhibits H^+ transfer [51]. When adding a small amount of composite catalyst Fe_2O_3@MWCNTs, the excellent adsorption performance of CNTs will adsorb a part of NH_3 to delay this 'deactivation'. That is why the low-decomposition temperature of AP is delayed when the added amounts of composite catalyst are 1 and 2%. However, CNTs have extraordinary physical and chemical properties, and excellent electric and thermal conductivity. Fe_2O_3 is a transition metal oxide and N-semiconductor with many valence states. Owing to their exceptional electronic characteristics

Table 2 Thermal decomposition kinetic parameters of samples

Samples	E_a, kJ/mol	LnA
a (0 wt%)	310.3	84.0
e (10 wt%)	81.4	29.3

Note: E_a is the thermal decomposing activation energy (kJ/mol) and A is the pre-exponential factor.

composite catalysts could offer accelerated electrons, speeding up the decomposition processes [52] and the oxidation–reduction process [53]. In addition, CNTs with excellent adsorption performance can adsorb $HClO_4$, which can form a metal perchloride compound with Fe_2O_3. This compound is very unstable and easily decomposes, and will decrease the E_a of AP [54]. What is more, Fe_2O_3 evenly dispersed in MWCNTs can offer more effective active sites for decomposition, thus further accelerating the catalysis process. So, with the increase in the amount of Fe_2O_3@MWCNTs used, the decomposition temperature of AP gradually decreases.

4. Conclusion: A simple physical absorption method is used to prepare Fe_2O_3@MWCNTs nanocomposites. This wet filling method is mild and superior. Using this method can obtain a high fill rate of the samples. The obtained Fe_2O_3@MWCNTs nanocomposites with smooth surfaces are uniformly filled by 25.8 wt% Fe_2O_3. Based on the visual inspection of all TEM images, the filling yield was estimated to be ca. 90%, higher than that of previous work [43]. The Fe_2O_3@MWCNTs composite material exhibits excellent catalytic performance on the thermal decomposition of AP, compared with that of the samples containing simple mixtures of Fe_2O_3 + AP, MWCNTs + AP and Fe_2O_3 + MWCNTs + AP. After adding 10% Fe_2O_3@MWCNTs, the peak temperature of AP decomposition decreased by 116°C compared with AP, and the amount of AP heat release increased about 200 kJ/mol. The E_a of AP had reduced from 310.3 to 81.4 kJ/mol. Using this method not only improves the dispersion of Fe_2O_3 nanoparticles, but also obtains a good catalytic effect on the thermal decomposition behaviour of AP. This will make better use of the MWCNTs and Fe_2O_3 in catalytic science. Moreover, it may also be useful in various important applications in nanotechnology, biomedical sciences and memory device technology.

5. Acknowledgments: This work is financially supported by the open fund of the State Key Laboratory Cultivation Base for Nonmetal Composites and Functional Materials of Sichuan Province (No. 11ZXFK26).

6 References

[1] Jiang W., Liu J., Liu Y., Cui P., Li F.: 'Preparation of Fe_2O_3/CNTs composites and its catalysis on thermal decomposition of AP', *J. Solid Rocket Technol.*, 2008, **31**, (1), pp. 65–68,78

[2] Shusser M., Culick F.E.C., Cohen N.S.: 'Combustion response of ammonium perchlorate composite propellants', *J. Propuls. Power*, 2002, **18**, (5), pp. 1093–1100

[3] Jacobs P.W.M., Whitehead H.M.: 'Decomposition and combustion of ammonium perchlorate', *Chem. Rev.*, 1969, **69**, (4), pp. 551–590

[4] Fitzgerald R.P., Brewster M.Q.: 'Flame and surface structure of laminate propellants with coarse and fine ammonium perchlorate', *Combust. Flame*, 2004, **136**, (3), pp. 313–326

[5] Liu J., Li F., Chen A., Yang Y., Ma Z.: 'Preparation of Fe_2O_3 nanoparticles and its catalytic effect on thermal decomposition of ammonium perchlorate (AP)', *J. Propuls. Technol.*, 2006, **27**, (4), pp. 381–384

[6] Ma Z., Li F., Chen A., Bai H.: 'Preparation and thermal decomposition behavior of Fe_2O_3/ammonium perchlorate composite nanoparticles', *Acta Chim. Sinica*, 2004, **62**, (13), pp. 1252–1255

[7] Cui P., Li F., Zhou J., Jiang W.: 'Preparation of Cu/Cnt composite particles and catalytic performance on thermal decomposition of ammonium perchlorate', *Propellants Explosives Pyrotech.*, 2006, **31**, (6), pp. 452–455

[8] Pascual J., Mendez J., Gomez-Herrero J., *ET AL.*: 'Properties of metallic nanowires: from conductance quantization to localization', *Science*, 1995, **267**, (5205), pp. 1793–1795

[9] Collins P.G., Zettl A., Bando H., Thess A., Smalley R.: 'Nanotube nanodevice', *Science*, 1997, **278**, (5335), pp. 100–102

[10] Dong X., Zhang Z., Jin S., *ET AL.*: 'Characterization of Fe–Ni (C) nanocapsules synthesized by arc discharge in methane', *J. Mater. Res.*, 1999, **14**, (5), pp. 1782–1790

doi: 10.1049/mnl.2014.0263

[11] Zhang Z., Zheng J., Skorvanek I., *ET AL.*: 'Shell/core structure and magnetic properties of carbon-coated Fe-Co (C) nanocapsules', *J. Phys., Condens. Matter*, 2001, **13**, (9), p. 1921
[12] Zhang Z., Yu J., Zheng J., *ET AL.*: 'Structure and magnetic properties of boron-oxide-coated Fe(B) nanocapsules prepared by arc discharge in diborane', *Phys. Rev. B*, 2001, **64**, (2), p. 024404
[13] Bubke K., Gnewuch H., Hempstead M., Hammer J., Green M.L.: 'Optical anisotropy of dispersed carbon nanotubes induced by an electric field', *Appl. Phys. Lett.*, 1997, **71**, (14), pp. 1906–1908
[14] Liu C., Fan Y., Liu M., Cong H., Cheng H., Dresselhaus M.S.: 'Hydrogen storage in single-walled carbon nanotubes at room temperature', *Science*, 1999, **286**, (5442), pp. 1127–1129
[15] Misewich J., Martel R., Avouris P., Tsang J., Heinze S., Tersoff J.: 'Electrically induced optical emission from a carbon nanotube FET', *Science*, 2003, **300**, (5620), pp. 783–786
[16] Bachtold A., Hadley P., Nakanishi T., Dekker C.: 'Logic circuits with carbon nanotube transistors', *Science*, 2001, **294**, (5545), pp. 1317–1320
[17] Vigolo B., Pénicaud A., Coulon C., *ET AL.*: 'Macroscopic fibers and ribbons of oriented carbon nanotubes', *Science*, 2000, **290**, (5495), pp. 1331–1334
[18] Kong J., Franklin N., Zhou C., *ET AL.*: 'Nanotube molecular wires as chemical sensors', *Science*, 2000, **287**, pp. 622–625
[19] Ebbesen T.W.: 'Carbon nanotubes', *Phys. Today*, 1996, **49**, (6), pp. 26–35
[20] Mönch I., Meye A., Leonhardt A., *ET AL.*: 'Ferromagnetic filled carbon nanotubes and nanoparticles: synthesis and lipid-mediated delivery into human tumor cells', *J. Magn. Magn. Mater.*, 2005, **290**, pp. 276–278
[21] Okuyama F., Hayashi T., Fujimoto Y.: 'Formation of carbon nanotubes and their filling with metallic fibers on ion-emitting field anodes', *J. Appl. Phys.*, 1998, **84**, (3), pp. 1626–1631
[22] Chou S.Y., Wei M.S., Krauss P.R., Fischer P.B.: 'Single-domain magnetic pillar array of 35 nm diameter and 65 Gbits/in.^{2} density for ultrahigh density quantum magnetic storage', *J. Appl. Phys.*, 1994, **76**, (10), pp. 6673–6675
[23] Scott J.H.J., Majetich S.A.: 'Morphology, structure, and growth of nanoparticles produced in a carbon arc', *Phys. Rev. B*, 1995, **52**, (17), p. 12564
[24] Seraphin S., Zhou D., Jiao J.: 'Filling the carbon nanocages', *J. Appl. Phys.*, 1996, **80**, (4), pp. 2097–2104
[25] Majetich S., Artman J., McHenry M., Nuhfer N., Staley S.: 'Preparation and properties of carbon-coated magnetic nanocrystallites', *Phys. Rev. B*, 1993, **48**, (22), p. 16845
[26] Hang B.T., Hayashi H., Yoon S.-H., Okada S., Yamaki J.: 'Fe_2O_3-filled carbon nanotubes as a negative electrode for an Fe–air battery', *J. Power Sources*, 2008, **178**, (1), pp. 393–401
[27] Wu W., Zhu Z., Liu Z., Xie Y., Zhang J., Hu T.: 'Preparation of carbon-encapsulated iron carbide nanoparticles by an explosion method', *Carbon*, 2003, **41**, (2), pp. 317–321
[28] Huo J., Song H., Chen X.: 'Preparation of carbon-encapsulated iron nanoparticles by co-carbonization of aromatic heavy oil and ferrocene', *Carbon*, 2004, **42**, (15), pp. 3177–3182
[29] Yu F., Wang J., Sheng Z., Su L.: 'Synthesis of carbon-encapsulated magnetic nanoparticles by spray pyrolysis of iron carbonyl and ethanol', *Carbon*, 2005, **43**, (14), pp. 3018–3021
[30] Liu S., Wehmschulte R.J.: 'A novel hybrid of carbon nanotubes/iron nanoparticles: iron-filled nodule-containing carbon nanotubes', *Carbon*, 2005, **43**, (7), pp. 1550–1555
[31] Kim H., Sigmund W.: 'Iron particles in carbon nanotubes', *Carbon*, 2005, **43**, (8), pp. 1743–1748
[32] Müller C., Hampel S., Elefant D., *ET AL.*: 'Iron filled carbon nanotubes grown on substrates with thin metal layers and their magnetic properties', *Carbon*, 2006, **44**, (9), pp. 1746–1753
[33] Huo J., Song H., Chen X., Lian W.: 'Formation and transformation of carbon-encapsulated iron carbide/iron nanorods', *Carbon*, 2006, **44**, (13), pp. 2849–2852
[34] Jain D., Wilhelm R.: 'An easy way to produce α-iron filled multi-walled carbon nanotubes', *Carbon*, 2007, **45**, (3), pp. 602–606
[35] Borowiak-Palen E., Mendoza E., Bachmatiuk A., *ET AL.*: 'Iron filled single-wall carbon nanotubes – a novel ferromagnetic medium', *Chem. Phys. Lett.*, 2006, **421**, (1–3), pp. 129–133
[36] Schnitzler M.C., Oliveira M.M., Ugarte D., Zarbin A.J.G.: 'One-step route to iron oxide-filled carbon nanotubes and bucky-onions based on the pyrolysis of organometallic precursors', *Chem. Phys. Lett.*, 2003, **381**, (5–6), pp. 541–548
[37] Jorge J., Flahaut E., Gonzalez-Jimenez F., *ET AL.*: 'Preparation and characterization of A-Fe nanowires located inside double wall carbon nanotubes', *Chem. Phys. Lett.*, 2008, **457**, (4), pp. 347–351
[38] Preckel R.F.: 'Plateau ballistics in nitrocellulose propellants', *AIAA J.*, 1965, **3**, (2), pp. 346–347
[39] Shukla M.K., Leszczynski J.: 'A density functional theory study on the effect of shape and size on the ionization potential and electron affinity of different carbon nanostructures', *Chem. Phys. Lett.*, 2006, **428**, (4–6), pp. 317–320
[40] Baughman R.H., Zakhidov A.A., de Heer W.A.: 'Carbon nanotubes – the route toward applications', *Science*, 2002, **297**, (5582), pp. 787–792
[41] Mench M., Yeh C., Kuo K.: 'Propellant burning rate enhancement and thermal behavior of ultra-fine aluminum powders (Alex)', *Energetic Materials: Production, Processing and Characterization*, Proc. 29th International Conf. of ICT, Karlsruhe, Germany, 1998, pp. 30–31
[42] Tan F., Fan X., Zhang G., Zhang F.: 'Coating and filling of carbon nanotubes with homogeneous magnetic nanoparticles', *Mater. Lett.*, 2007, **61**, (8–9), pp. 1805–1808
[43] Tilmaciu C.-M., Soula B., Galibert A.-M., *ET AL.*: 'Synthesis of superparamagnetic iron(III) oxide nanowires in double-walled carbon nanotubes', *Chem. Commun.*, 2009, **2009**, (43), pp. 6664–6666
[44] Liu Z., Li X., Liu Z., Lu J.: 'Synthesis and catalytic behaviors of cobalt nanocrystals with special morphologies', *Powder Technol.*, 2009, **189**, (3), pp. 514–519
[45] Chaturvedi S., Dave P.N.: 'A review on the use of nanometals as catalysts for the thermal decomposition of ammonium perchlorate', *J. Saudi Chem. Soc.*, 2013, **17**, (2), pp. 135–149
[46] Duan G., Yang X., Chen J., Huang G., Lu L., Wang X.: 'The catalytic effect of nanosized MgO on the decomposition of ammonium perchlorate', *Powder Technol.*, 2007, **172**, (1), pp. 27–29
[47] Wang B., Feng Z., Yang R.: 'Theory on combustion of explosives and propellants' (Beijing Institute of Technology Press, 1997)
[48] Yun Z., Zhou Z.: 'Thermal analysis kinetics data processing', *Chin. J. Explosives Propellants*, 1983, (2), pp. 24–35
[49] Cui P., Li F., Zhou J., Jiang W., Yang Y.: 'Preparation of Cu/CNTs composite particles and thermal decomposition behavior of ammonium perchlorate', *J. Inorganic Mater.*, 2006, **21**, (2), pp. 303–308
[50] Devi T.G., Kannan M.P., Hema B.: 'Thermal decomposition of cubic ammonium perchlorate – the effect of barium doping', *Thermochim. Acta*, 1996, **285**, (2), pp. 269–276
[51] Liu Z., Yin C., Kong Y., Zhao F., Luo Y., Xiang H.: 'The thermal decomposition of ammonium perchlorate', *Energetic Mater.*, 2000, **8**, (2), pp. 75–79
[52] Li N., Geng Z., Cao M., *ET AL.*: 'Well-dispersed ultrafine MN_3O_4 nanoparticles on graphene as a promising catalyst for the thermal decomposition of ammonium perchlorate', *Carbon*, 2013, **54**, pp. 124–132
[53] Rudloff W.K., Freeman E.S.: 'Catalytic effect of metal oxides on thermal decomposition reactions. II. Catalytic effect of metal oxides on the thermal decomposition of potassium chlorate and potassium perchlorate as detected by thermal analysis methods', *J. Phys. Chem.*, 1970, **74**, (18), pp. 3317–3324
[54] Yin C., Liu Z., Kong Y., Zhao F., Luo Y.: 'The catalyzed decomposition of ammonium perchlorate'. 10th National Symp. on Chemical Thermodynamics and Thermal Analysis, Chinese Chemical Society, 2000